

Prescribing Patterns in Growing Tubular Soft Matter by Initial Residual Stress

Yangkun Du,^{a,b} Chaofeng Lü,^{c,d,e,‡} Congshan Liu,^c Zilong Han,^a Jian Li,^a Weiqiu Chen,^{a,d,e} Shaoxing Qu,^{a,d,e} and Michel Destrade^{b,a}

Initial residual stress is omnipresent in biological tissues and soft matter, and can affect growth-induced pattern selection significantly. Here we demonstrate this effect experimentally by letting gel tubes grow in the presence or absence of initial residual stress and by observing different growth pattern evolutions. These experiments motivate us to model the mechanisms at play when a growing bilayer tubular organ spontaneously displays buckling patterns on its inner surface. We demonstrate that not only differential growth, geometry and elasticity, but also initial residual stress distribution, exert a notable influence on these pattern phenomena. Prescribing an initial residual stress may offer an alternative or a more effective way to implement a pattern selection for growable bio-tissues or soft matter. The results also show promise for the design of 4D bio-mimic printing protocols or for controlling hydrogel actuators.

1 Introduction

Pattern creation in soft solids is a common phenomenon in Nature and is now being promoted in biomedical and industrial applications. In biological systems, some specific patterns are used to maintain essential bio-functions such as the wrinkles found in the intestine (Fig. 1A), useful for digesting, and the interconnected creases of the brain cortex, associated with intelligence development^{1,2}. Other patterns are used to transmit pathological changes: hence, an abnormally wrinkled airway indicates asthmatic bronchiole, and frequent morphological changes of a tumor point to a pre-metastatic state³. In other words, Nature and Evolution have mastered well how to control and select optimal patterns for soft tissues. In turn, engineers try to mimic these processes to recreate and control ideal patterns in manufacturing. For example, self-assembly of a substrate-film structure for 3D micro-fabrication is achieved by local mismatch deformation between substrate and film: the resulting substrate curvature underpins spontaneous micro- or nano-patterns and structures⁴⁻⁶. Similarly, stimuli-responsive hydrogel actuators can be designed by prescribing inhomogeneous swelling and made to wrinkle into different patterns.

Physically, wrinkle/crease patterns are created by mechanically-induced instability and post-buckling process. The special case of spontaneous instability and post-buckling in the absence of external loads can be explained by the presence of inhomogeneous *residual stress fields*. These have

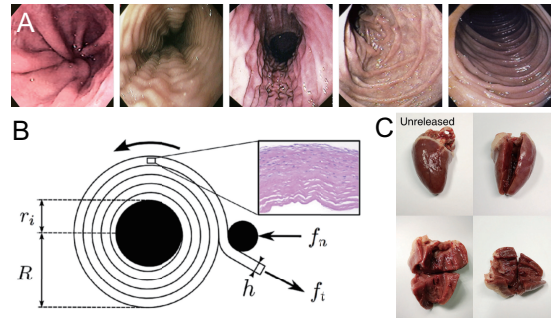


Fig. 1 (A) Different morphological wrinkling patterns along the human intestine⁷; (B) A protocol for printing non-Euclidean solids, similar to 3D-printing bio-tissues in bioengineering⁸; (C) Residual stresses can be released in a duck heart by cutting it in different directions⁹.

been demonstrated experimentally for many bio-tissues such as skin, arteries, heart, brain, intestine, solid tumors, etc.^{1,10-15}, where they are required to ensure self-equilibrium, transfer bio-signals, or maintain some specific bio-functions¹⁶⁻¹⁸. They can also endow elastic materials with prescribed properties (Fig. 1B). A strong effort has been dedicated to model growth-induced residual stresses and the resulting pattern-generating instability^{1,19-22}. These papers used volume growth theory²³, where growth is initiated from an initially stress-free configuration. In particular, the influence of differential volume growth and growth velocity on the creation of residual stress in bilayer cylinders was elucidated, resulting in a pattern selection protocol which can be tuned by changing thickness and stiffnesses ratios^{1,23-25}.

However, most living tissues do not possess a stress-free initial configuration, as can be checked by cutting them in different directions: each cut releases some residual stress and consequently an infinite number of cuts are required to attain this hypothetical zero stress initial configuration (see the examples of a cut duck heart in Fig. 1B or cut human arteries in¹⁰). In real-

^a Department of Engineering Mechanics, Zhejiang University, Hangzhou, P. R. China;

^b School of Mathematics, Statistics and Applied Mathematics, NUI Galway, Galway, Ireland;

^c Department of Civil Engineering, Zhejiang University, Hangzhou 310058, P.R. China;

^d Key Lab of Soft Machines and Smart Devices of Zhejiang Province, Zhejiang University, Hangzhou, P.R. China;

^e Soft Matter Research Center, Zhejiang University, Hangzhou 310027, P. R. China.

[‡] Fax: 86-571-8820-8685; Tel: 86-571-8820-8473; E-mail: lucf@zju.edu.cn

ity, long-term growth and remodelling processes and other bio-interactions are impossible to track and reconstruct for living matter. Hence, the stress-free assumption for the initial state is too strong, and neglecting initial residual stress may affect the analysis of growth-induced residual stress and the resulting pattern selection, as we have proofed in our previous paper²⁶ on the growth human aorta with different initial residual stress.

In this current paper, we designed an experiment with swelling hydrogel and different residual stresses preset by shrink-fitting way to demonstrate the influence of initial residual stress on growth and the significance of our series works. Furthermore, by simplifying the initial radial stress as linear distribution with a magnitude factor instead of the specific and complex residual stress distribution, we are able to recover qualitatively all possible residual stress distributions. Both the experimental and theoretical results have the consistent conclusions that the initial residual stress will not only affect the growth-induced residual stress and the pattern evolution but also do impact the onset of the critical buckling which is very important in practice.

We structure this paper as follow. In Section 2, we show the experiment process and the pattern evolution phenomenons which assess the significance of the initial residuals on growth and morphologies. Section 3 is about the mathematical modelling on growth and instability analysis corresponding to the experiment. Also, the typical residual stress distribution is provided based on self-equilibrium and boundary conditions. In section 4 and 5, we disclose some results and conclusions.

2 Experiments

Here, we designed an experiment to illustrate the influence of the initial residual stress on the growth-induced pattern evolutions. We use the shrink-fitting way to prescribe the initial residual stress into the bilayer structures which are made of the hydrogel inside and rubber outside. The hydrogel here is used to simulate the isotropic growth process.

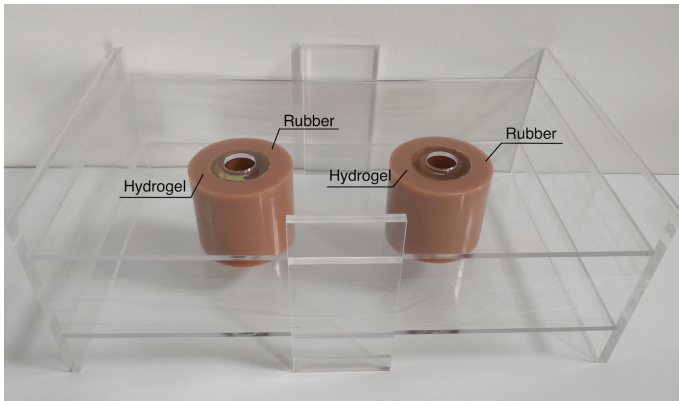


Fig. 2 Experimental equipment for isotropic growth-induced instability of bilayer tubes, one with non-zero initial residual stress, one without.

2.1 Protocol

First, we prescribed an initial residual stress by setting an incompatible geometry for the two separate parts (hydrogel and rubber). We preset the outer radius of the inner layer hydrogel to be a little larger than the inner radius of the outer layer rubber. Then, by shrink-fitting the hydrogel into the rubber, we

created a compressive hoop stress in the hydrogel and a tensile hoop stress in the rubber. We measured the changes in radii due to the shrink-fitting and found them to be negligible (less than 1 mm).

For direct comparison with the case where there is no initial stress, we nested another hydrogel tube into another rubber tube, with the same geometry and materials as the first bilayer tube, but no incompatibility (the outer radius of the hydrogel was equal to the inner radius of the rubber).

All tubes were 7 cm tall. The inner hydrogel tubes had inner radius $R_i = 30$ mm and outer radius $R_s = 45$ mm. The outer rubber tubes had inner radius $R_s = 45$ mm and outer radius $R_o = 80$ mm. The elastic modulus of inert rubber is 448 kPa, while the elastic modulus of swelling hydrogel is 87 kPa.

We placed the two bilayer tubes in an Acrylic frame, with fixed top and bottom plates, to constrain the deformation in the axial direction, see the experimental equipment shown in Figure 2. We pierced two circular holes on both the top and bottom plates, with centres on the axis of the tubes, for water to flow freely during the growth period.

Finally, the frame and tubes were placed in a big water tank.

2.2 Materials

Hydrogel: N,NâĀŽ-methylenebis(Acrylamide) 98% (MBAA, Lot #146072) and Ammonium persulfate 98% (APS, Lot #248614) were purchased from Sigma-Aldrich; Acrylamide 99% (AAm, Lot #A108465) was purchased from Aladdin, Shanghai, China. All reagents were used as received.

Rubber: VytaFlexTM 30 was purchased from Smooth-On, Ma-cungie, USA.

2.3 Preparation

Hydrogel: First, the AAm monomer is dissolved in distilled water to form a solution of concentration 4 mol/L. Then, to every 1 ml of the solution, 4 μ l of a 0.1 mol/L of MBAA solution is added as the conventional cross-linker, and 20 μ l of a 0.1 mol/L ammonium persulfate solution is added as the UV initiator. The resulting solution is degassed by N₂ for 1 hour and then poured into a mould made of laser-cut acrylic sheets. The mould and the solution are covered with the bottom of a Petri dish to prevent oxygen inhibition. The covered mould is then placed under a UV lamp and exposed to UV irradiation (wavelength = 365 nm). Finally, the hydrogel is taken out of the mould and washed with de-ionized water thoroughly to remove any unreacted monomers, and is kept at room temperature.

Rubber: See the fabrication instructions at <http://www.smooth-on.com.cn/uploadfile/2018/0510/20180510040704891.pdf>

2.4 Experimental conclusions

Fig. 3 provides experimental proof of the impact of initial residual stress on growth-induced pattern creation and evolution. The two bilayer cylinders have the same geometry and materials but different initial residual stresses. The prescribed initial residual stresses are stress-free for one bilayer tube (Fig. 3A), and compressive hoop stress in hydrogel and tensile hoop stress in rubber for the other (Fig. 3B)

The results show that by prescribing an initial residual stress, we can bring forward the onset of instability and also create a

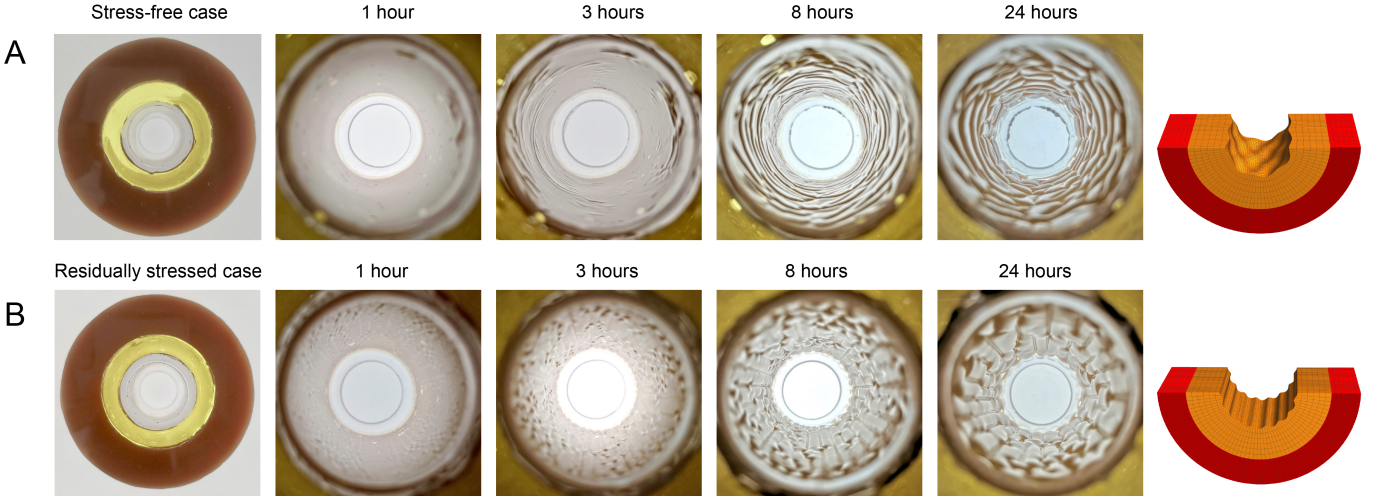


Fig. 3 Growth-induced buckling of bilayer tubes (inner layer: swelling hydrogel, outer layer: inert rubber) with (A) stress-free and (B) residually stressed initial states. By shrink-fitting, we created a non-zero initial residual stress in (B) (compressive hoop stress in the hydrogel, tensile hoop stress in the rubber). Otherwise, (A) and (B) have the same initial geometry and material parameters ($R_o/R_s \simeq 1.8$, $R_s/R_i = 1.5$, $\mu^{\text{inn}}/\mu^{\text{out}} \simeq 0.2$). Axial growth is prevented. Once submerged in water, (B) buckles earlier and in a different pattern (wrinkle-front aligned with the axis) than (A) (mixed axial/circumferential wrinkles).

pattern with straight circumferential folds along the axial direction, as opposed to the postponed, mixed circumferential and axial folds shown in Fig. 3A.

3 Modeling

3.1 Growth with initial residual stress

Here we show that the so-called ‘modified multiplicative decomposition growth’ (MMDG) model^{9,26} is consistent with our experimental findings.

The MMDG framework relies on the concept of multiplicative decomposition, similar to the conventional volumetric growth model²³. Its innovation lies in the introduction of an initial elastic deformation \mathbf{F}_0 which is used for releasing the initial residual stress to a virtual stress-free configuration. Thereafter, the independent unconstrained growth process \mathbf{F}_g can take place freely, using two virtual stress-free and incompatible configurations. The elastic deformation \mathbf{F}_e then makes the material compatible again. Accordingly, the total growth process can be formulated by the deformation gradient

$$\mathbf{F} = \mathbf{F}_e \mathbf{F}_g \mathbf{F}_0. \quad (1)$$

Here, we assume that the material in its virtual stress-free state is an incompressible neo-Hookean solid. Then the constitutive equation for isotropic growth is

$$\boldsymbol{\sigma} = J_g^{-\frac{2}{3}} \left(\mathbf{F} \boldsymbol{\tau} \mathbf{F}^T + p_0 \mathbf{F} \mathbf{F}^T \right) - p \mathbf{I}, \quad (2)$$

where p , p_0 are the Lagrange multipliers in current and reference configurations, respectively, and $J_g = \det \mathbf{F}_g$ tracks local volume change. The initial stress $\boldsymbol{\tau}$ and the Cauchy stress $\boldsymbol{\sigma}$ satisfy the equilibrium equations and boundary conditions in each configuration,

$$\text{Div } \boldsymbol{\tau} = \mathbf{0}, \quad \boldsymbol{\tau}^T \mathbf{N} = \mathbf{0}, \quad \text{div } \boldsymbol{\sigma} = \mathbf{0}, \quad \boldsymbol{\sigma}^T \mathbf{n} = \mathbf{0}, \quad (3)$$

where \mathbf{n} , \mathbf{N} are unit vectors normal to the boundary.

3.2 Geometry and initial residual stress field

For comparison with previous results on pattern selection in growing tubular soft solids²⁸, we characterise our bilayer tube as being typical of bio-tissues. Hence, we take shear moduli in the ranges $\mu^{\text{inn}} = 120 - 700$ Pa, $\mu^{\text{out}} = 1$ kPa (close to those of embryonic gastrointestinal tissue). We take the the outer layer radius $R_o = 1$, interface radius $R_s = R_o/1.8$ and inner radius R_i as a geometric variable.

To reproduce the initial residual stress in the experiments and in some bilayer tissues, we prescribe a linear variation of the radial initial residual stress, as

$$\begin{aligned} \tau_{RR}^{\text{inn}} &= \frac{\alpha}{R_s - R_i} (R - R_i), \\ \tau_{RR}^{\text{out}} &= \frac{\alpha}{R_o - R_i} (R - R_s), \end{aligned} \quad (4)$$

which satisfies the required boundary conditions at the inner (R_i), interface (R_s) and outer (R_o) surfaces of the bilayer. We take the axial initial residual stress as $\tau_{ZZ}^{\text{inn}} = \tau_{ZZ}^{\text{out}} = 0$. Then we obtain the distribution of the circumferential stress $\tau_{\theta\theta}$ by solving $\text{Div } \boldsymbol{\tau} = \mathbf{0}$, the self-equilibrium equation for the initial residual stress.

The initial residual stress field in Eq.(4) is compressive radial stress τ_{RR} and a hoop stress $\tau_{\theta\theta}$ which is compressive (tensile) in the inner (outer) layer, reproducing the qualitative characteristics of our experiments on hydrogel/rubber tubes. We pre-multiply this initial residual stress distribution by a magnitude factor α , which we use to quantify the influence of the initial stress: $\alpha = 0$ means a totally stress-free initial state, $\alpha > 0$ means the inner layer is under compressive hoop initial stress (as in our experiments), $\alpha < 0$ means the outer layer is hoop-compressed initially. Finally we call g^{inn} , g^{out} the volumetric growth factors in the inner and outer layers, respectively, and we solve the corresponding buckling boundary value problem.

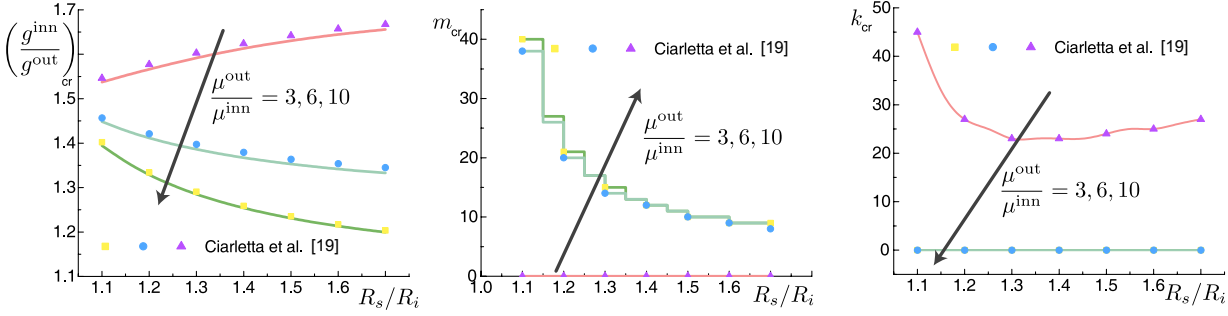


Fig. 4 Benchmark results of growth-induced instability without initial residual stress²⁸, where $R_o/R_s = 1.8$, $R_o = 1$, $g^{ad} = 1$.

3.3 Buckling analysis

The onset of instability is analyzed by relying on linear incremental theory³⁰ and on our previous papers^{9,26}.

In short, there exists a relation giving the increment $\dot{\mathbf{F}}$ of the displacement gradient \mathbf{F} with respect to the reference configuration as $\dot{\mathbf{F}} = \dot{\mathbf{F}}_I \mathbf{F}$, where $\dot{\mathbf{F}}_I$ is the incremental displacement gradient with respect to the current configuration. Since the growth process is assumed to be independent of the stress and strain fields due to the infinitesimal and transient incremental deformation, we also have the relationship $\dot{\mathbf{F}}_e = \dot{\mathbf{F}}_I \mathbf{F}_e$ for the pure elastic gradient \mathbf{F}_e and its increment.

By prescribing the incremental displacement field as

$$\dot{\mathbf{x}} = u(r, \theta, z) \mathbf{e}_r + v(r, \theta, z) \mathbf{e}_\theta + w(r, \theta, z) \mathbf{e}_z, \quad (5)$$

we get the incremental displacement gradient tensor as

$$\dot{\mathbf{F}}_I = \frac{\partial \dot{\mathbf{x}}}{\partial \mathbf{x}} = \begin{bmatrix} \frac{\partial u}{\partial r} & \frac{1}{r} \left(\frac{\partial u}{\partial \theta} - v \right) & \frac{\partial u}{\partial z} \\ \frac{\partial v}{\partial r} & \frac{1}{r} \left(\frac{\partial v}{\partial \theta} + u \right) & \frac{\partial v}{\partial z} \\ \frac{\partial w}{\partial r} & \frac{1}{r} \frac{\partial w}{\partial \theta} & \frac{\partial w}{\partial z} \end{bmatrix}. \quad (6)$$

Then the incremental incompressibility condition reads

$$\text{tr} \dot{\mathbf{F}}_I = \frac{\partial u}{\partial r} + \frac{1}{r} \left(\frac{\partial v}{\partial \theta} + u \right) + \frac{\partial w}{\partial z} = 0. \quad (7)$$

Now the incremental nominal stress $\dot{\mathbf{S}}$ in push-forward form has components

$$\dot{S}_{ij} = A^I_{eijkl} \dot{F}_{Ilk} - \dot{p} \delta_{ij} + p \dot{F}_{Iij}, \quad (8)$$

where $A^I_{eijkl} = F_{ei\alpha} F_{ek\beta} \frac{\partial \psi}{\partial F_{e\alpha\beta}}$ are the components of the instantaneous elasticity tensor, calculated by differentiating the strain energy density. Finally, the incremental stress equilibrium equations are:

$$\text{div} \dot{\mathbf{S}}_I = \mathbf{0}, \quad \dot{\mathbf{S}}_I^T \mathbf{n} = \mathbf{0}, \quad (9)$$

The forms of incremental displacement fields are specified as circumferential and axial sinusoidal wrinkles, in the form $[u, \dot{p}] = [U(r), Q(r)] \cos(m\theta) \cos(\kappa z)$, $v = V(r) \sin(m\theta) \cos(\kappa z)$, $w = W(r) \sin(m\theta) \cos(\kappa z)$, where m and $\kappa = 2\pi n/L$ are the circumferential and axial wave numbers, respectively. Then the incremental nominal stress components are similar, as $\dot{S}_{Irr} = \Sigma_{rr}(r) \cos(m\theta) \cos(\kappa z)$, $\dot{S}_{I\theta\theta} = \Sigma_{r\theta}(r) \sin(m\theta) \cos(\kappa z)$, $\dot{S}_{Irz} = \Sigma_{rz}(r) \cos(m\theta) \sin(\kappa z)$. Finally, we arrive at the Stroh formu-

lation of the incremental equations of equilibrium, as

$$\boldsymbol{\eta}(r) = [U(r), V(r), W(r), r\Sigma_{rr}(r), r\Sigma_{r\theta}(r), r\Sigma_{rz}(r)]^T,$$

$$\frac{d}{dr} \boldsymbol{\eta}(r) = \frac{1}{r} \begin{bmatrix} \mathbf{G}_1(r) & \mathbf{G}_2(r) \\ \mathbf{G}_3(r) & \mathbf{G}_4(r) \end{bmatrix} \boldsymbol{\eta}(r), \quad (10)$$

see^{9,26} for details.

Finally, by iterating over the wrinkle numbers m and n for the numerical solution of Eq. (10), we obtain the critical value of each case which creates a buckling pattern for some given differential growth ratio. Here, we use the surface impedance method to integrate the Stroh formulation^{31–34}.

4 Results

The numerical strategy is to find the smallest differential growth ratio $g^{\text{inn}}/g^{\text{out}}$ for which an incremental solution exists, for given wrinkle numbers n, m . Then after spanning all possible wrinkle numbers in the circumferential and axial directions, we keep the smallest ratio $(g^{\text{inn}}/g^{\text{out}})_{\text{cr}}$ for the onset of buckling. If the corresponding $n_{\text{cr}}, m_{\text{cr}}$ are both non-zero, then the wrinkling pattern is two-dimensional.

According to the expression of the initial residual stress in Eq. (4), we can recover instability results with a stress-free initial state by prescribing $\alpha = 0$, and use the results as benchmark results, see Figure 4. Hence we see that increasing the thickness or stiffness ratio of the outer to inner tubes will create fewer folds in the circumferential direction and more folds in the axial direction. A deep analysis of pattern selection by these factors has been conducted by Ciarletta *et al.*²⁸.

In that case, which is not realistic for actual living matter (Fig. 1B), pattern selection can only be tuned by the geometric and elastic parameters. Starting then from an initially stressed state $\alpha \neq 0$, we find that pattern selection can be largely tuned or prescribed by the magnitude α of the initial stress $\boldsymbol{\tau}$.

Generally, soft tubular tissues are too soft to sustain increasing levels of initial residual stresses for long, especially compressive hoop stresses, which quickly induce buckling patterns in the absence of growth $((g^{\text{in}}/g^{\text{ad}})_{\text{cr}} = 1)$ and external loads³⁵. Here we find that this occurs when the amplitude of the initial stress is large enough. Hence, wrinkles appear on the inner face of the composite tube when $\alpha > \alpha_{\text{upp}} \simeq 1.003$, and on its outer face when $\alpha < \alpha_{\text{low}} \simeq -4.560$ (as the outer layer is then under large compressive hoop stress), see Fig. 5.

Otherwise, when $\alpha_{\text{low}} < \alpha < \alpha_{\text{upp}}$, instability is due to combined high levels of initial stress and differential growth. Figs. 5 and 6 show the effect of the initial stress magnitude α on the

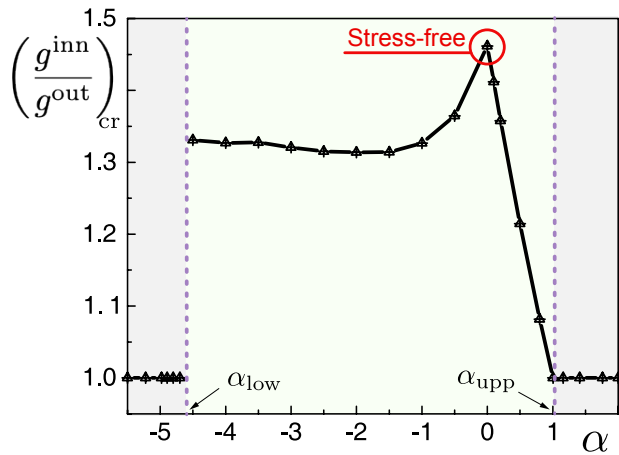


Fig. 5 Variation of the critical differential growth ratio $(g^{\text{inn}}/g^{\text{out}})_{\text{cr}}$ with the level of initial stress α , when the stiffness ratio is $\mu^{\text{inn}}/\mu^{\text{out}} = 1/5$.

evolution of growth-induced patterns. Fig. 5 shows that with initial residual stress ($\alpha \neq 0$), the level of differential growth $(g^{\text{inn}}/g^{\text{out}})_{\text{cr}}$ required for buckling is reduced. It is worth noting here that this calculation result is consistent with our experimental finding in Fig. 3 that the stress-free case occurs wrinkles earlier than the residual stress case.

Fig. 6 gives the numbers of circumferential and axial wrinkles. In the pure growth-induced case ($\alpha = 0$), a 2D-pattern is predicted ($m_{\text{cr}} = 7$, $n_{\text{cr}} = 2$), consistent with our experiments (Fig. 3A). Then, increasing the initial circumferential compressive stress in the inner layer with $\alpha > 0$ increases m_{cr} and decreases n_{cr} . Quickly (see zoom of the $-0.1 < \alpha < 0.1$ range in Fig. 6B), $n_{\text{cr}} = 0$ and the wrinkles are aligned with the tube axis, consistent with our experiments (Fig. 3B). Conversely, reversing the location of circumferential compressive and tensile stresses by taking $\alpha < 0$ leads to $m_{\text{cr}} = 0$. Fig. 6B further displays the details and profiles of possible patterns around $\alpha = 0$, and shows how sensitive they are to initial residual stress. Effectively, all the wrinkling scenarios encountered in the intestine (Fig. 1A) can be captured by varying the magnitude and the sign of α only, while keeping the geometric and material parameters the same throughout. The figures demonstrate how to obtain, control and advance pattern creation by prescribing initial residual stress fields for given elasticities and geometries.

5 Conclusions

We investigated the natural capability of biological tubular tissues to use initial residual stresses to control pattern creation, based on a recently developed growth model, and also mimicked the results experimentally by swelling hydrogel tubes. Initial stress is an effective and controllable factor for pattern selection beyond the geometric and elastic parameters highlighted in previous studies of pure growth²⁸. We also showed that there is an effective range $\alpha_{\text{low}} < \alpha < \alpha_{\text{upp}}$ for the level of initial stress where patterns can be prescribed on growable bio-tissues. We did not expand the instability analysis beyond the linearised buckling state, but it is worth noting that wrinkles are very stable for layered structures and give the number and wavelength of the eventual super-critical creases³⁶. They are also a way to measure the level of a known distribution of

initial stress³⁵.

Our hope is that these results may provide an inspiring insight for directional bionic self-assembly or robot manufacturing by initial residual stress.

References

- 1 V. Balbi, E. Kuhl and P. Ciarletta, *J. Mech. Phys. Solids*, 2015, **78**, 493–510.
- 2 J. Altman and S. A. Bayer, *The human brain during the second trimester*, CRC Press, 2005.
- 3 E. T. Roussos, J. S. Condeelis and A. Patsialou, *Nat. Rev. Cancer*, 2011, **11**, 573 EP –.
- 4 J. Yin, E. Bar-Kochba and X. Chen, *Soft Matter*, 2009, **5**, 3469–3474.
- 5 X. Chen and J. Yin, *Soft Matter*, 2010, **6**, 5667–5680.
- 6 X. Chen, *Mechanical Self-Assembly: Science and Applications*, Springer Science & Business Media, 2012.
- 7 C. M. Wilcox, M. Muñoz-Navas and J. J. Sung, *Atlas of Clinical Gastrointestinal Endoscopy E-Book: Expert Consult-Online and Print*, Elsevier Health Sciences, 2012.
- 8 G. Zurlo and L. Truskinovsky, *Phys. Rev. Lett.*, 2017, **119**, 048001.
- 9 Y. Du, C. Lü, W. Chen and M. Destrade, *J. Mech. Phys. Solids*, 2018, **118**, 133–151.
- 10 G. A. Holzapfel, G. Sommer, M. Auer, P. Regitnig and R. W. Ogden, *Ann. Biomed. Eng.*, 2007, **35**, 530–545.
- 11 G. A. Holzapfel and R. W. Ogden, *J. Royal Soc. Interface*, 2010, **7**, 787–799.
- 12 J. H. Omens and Y.-C. Fung, *Circ. Res.*, 1990, **66**, 37–45.
- 13 T. Savin, N. A. Kurpios, A. E. Shyer, P. Florescu, H. Liang, L. Mahadevan and C. J. Tabin, *Nature*, 2011, **476**, 57–62.
- 14 T. Stylianopoulos, J. D. Martin, V. P. Chauhan, S. R. Jain, B. Diop-Frimpong, N. Bardeesy, B. L. Smith, C. R. Ferrone, F. J. Hornicek, Y. Boucher, L. L. Munn and R. K. Jain, *Proc. Natl. Acad. Sci. U.S.A.*, 2012, **109**, 15101–15108.
- 15 M. E. Fernandez-Sanchez, S. Barbier, J. Whitehead, G. Bealle, A. Michel, H. Latorre-Ossa, C. Rey, L. Fouassier, A. Claperon, L. Brulle, E. Girard, N. Servant, T. Rio-Frio, H. Marie, S. Lesieur, C. Housset, J. L. Gennisson, M. Tanter, C. Menager, S. Fre, S. Robine and E. Farge, *Nature*, 2015, **523**, 92–95.
- 16 Y. Pan, I. Heemskerk, C. Ibar, B. I. Shraiman and K. D. Irvine, *Proc. Natl. Acad. Sci. U.S.A.*, 2016, 201615012.
- 17 T. P. Padera, B. R. Stoll, J. B. Tooredman, D. Capen, E. D. Tomaso and R. K. Jain, *Nature*, 2004, **427**, 695.
- 18 G. Helmlinger, P. A. Netti, H. C. Lichtenbeld, R. J. Melder and R. K. Jain, *Nat. Biotechnol.*, 1997, **15**, 778.
- 19 Y.-P. Cao, B. Li and X.-Q. Feng, *Soft Matter*, 2012, **8**, 556–562.
- 20 B. Li, Y.-P. Cao, X.-Q. Feng and H. Gao, *J. Mech. Phys. Solids*, 2011, **59**, 758–774.
- 21 C. Lü and Y. Du, *Int. J. Appl. Mech.*, 2016, **8**, 1640010.
- 22 Y. Du and C. Lü, *Theor. Appl. Mech. Lett.*, 2017, **7**, 117–120.
- 23 E. K. Rodriguez, A. Hoger and A. D. McCulloch, *J. Biomech.*, 1994, **27**, 455–467.
- 24 A. Goriely and M. Ben Amar, *Phys. Rev. Lett.*, 2005, **94**, 198103.
- 25 P. Ciarletta, *Phys. Rev. Lett.*, 2013, **110**, 158102.

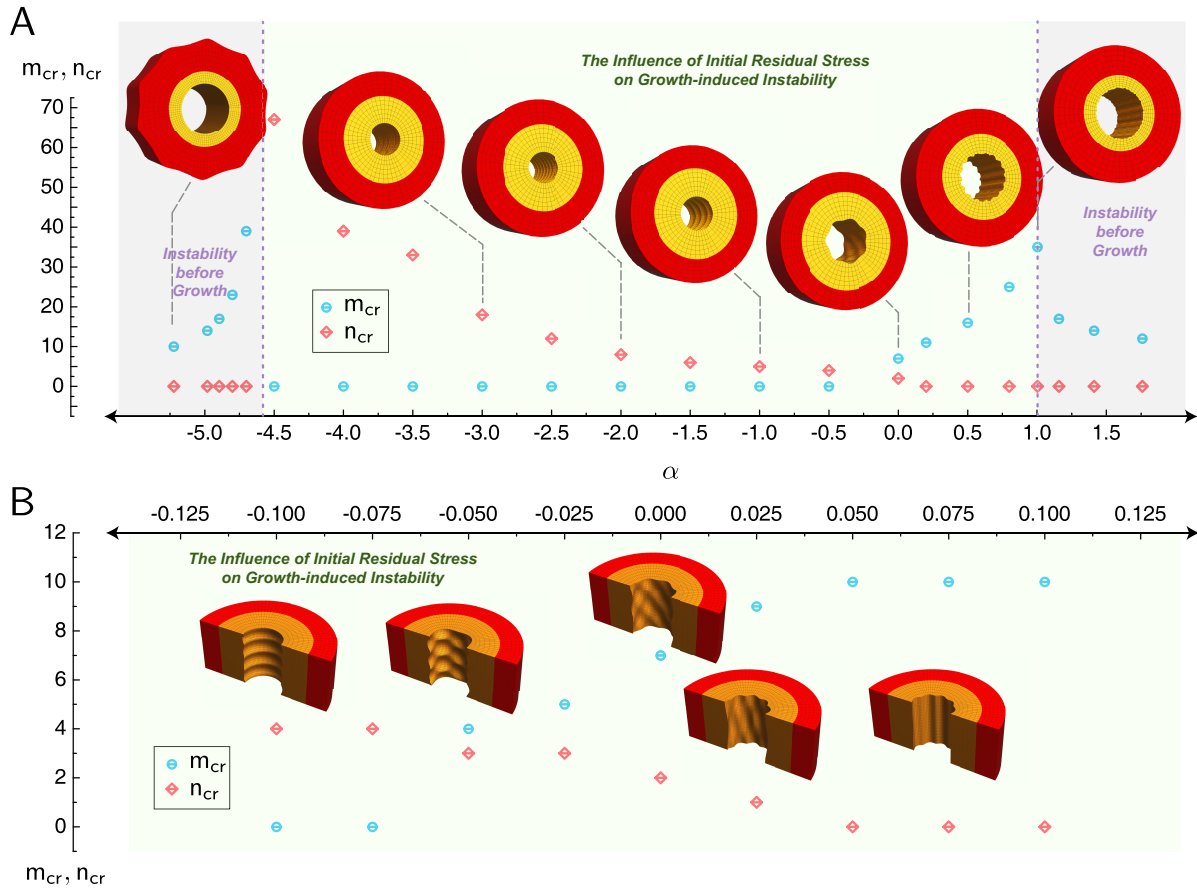


Fig. 6 (A) Effect of the magnitude of the initial residual stresses α on growth-induced pattern selection, when $\mu^{inn}/\mu^{out} = 1/5$; (B) Zoom of the results in the range $-0.01 < \alpha < 0.01$ in (A).

- 26 Y. Du, C. Lü, W. Chen and M. Destrade, *Sc. Reports*, 2019, **9**, 8232.
- 27 S. Sadik and A. Yavari, *Math. Mech. Solids*, 2015, **22**, 771–772.
- 28 P. Ciarletta, V. Balbi and E. Kuhl, *Phys. Rev. Lett.*, 2014, **113**, 248101.
- 29 P. Pedersen, *Computational Mechanics*, 2006, **37**, 121–130.
- 30 R. W. Ogden, *Non-linear elastic deformations*, Courier Corporation, 1997.
- 31 S. Biryukov, *Sov. Phys. Acoust.*, 1985, **31**, 350–354.
- 32 M. Destrade, J. Murphy and R. Ogden, *Int. J. Eng. Sci.*, 2010, **48**, 1212 – 1224.
- 33 M. Destrade, A. Ní Annaidh and C. D. Coman, *Int. J. Solids Struct.*, 2009, **46**, 4322 – 4330.
- 34 Y. Su, B. Wu, W. Chen and M. Destrade, *J. Mech. Phys. Solids*, 2019.
- 35 P. Ciarletta, M. Destrade, A. L. Gower and M. Taffetani, *J. Mech. Phys. Solids*, 2016, **90**, 242–253.
- 36 Y. Cao and J. W. Hutchinson, *Proc. Roy. Soc. A*, 2011, **468**, 94–115.